PROCEEDINGS OF SPIE

SPIEDigitalLibrary.org/conference-proceedings-of-spie

Impact of the necking phenomenon on the spectral behavior of WO< sub>3</sub> aggregates

Krzysztof Skorupski

SPIE.

Impact of the necking phenomenon on the spectral behavior of WO_3 aggregates

Krzysztof Skorupski

Wroclaw University of Science and Technology, Chair of Electronics and Photonics Metrology, Boleslawa Prusa 53/55, 50-317 Wroclaw, Poland

ABSTRACT

Fractal-like aggregates are usually modeled as monodisperse particles positioned in point contact. However, in reality, much more advanced connections between primary particles exist. In this work, new parameters for measuring both the intersection level and the neck level were introduced. Then, the impact of the connection type on the spectral behavior of fractal-like WO_3 aggregates was studied. For light scattering simulations, in the visible spectrum, the ADDA algorithm was used. The results prove that necks have strong impact on the spectral behavior of WO_3 aggregates and connections, which exist between primary particles, should not be excluded from models.

Keywords: Light scattering, Fractal-like aggregates, Discrete Dipole Approximation, WO3, Sintering, Necking

1. INTRODUCTION

Small particles, soon after emission, tend to connect to each other and create large geometries, namely aggregates. These geometries reveal some of the fractal properties, and therefore, can be described by the following equation:[1,2]

$$N_p = k_f \left(\frac{R_g}{r_p} \right)^{D_f}, \tag{1}$$

in which N_p defines the number of monodisperse primary particles and r_p stands for their radius. D_f and k_f are the fractal dimension and the fractal prefactor respectively. Finally, R_g denotes the radius of gyration.

Generally, fractal-like aggregates are modeled as assemblies of monodisperse primary particles positioned in point contact.[3] However, this is just a rough approximation. For example, a fraction of the volume might be transferred from the particle surface to the nearest connection point and create a much more stable, complex bond.[4] This work was focused on two physical phenomena, namely the adhesion and the densification. They both can be used to enhance fractal-like aggregate models. The first one defines all processes that affect the aforementioned volume transfer. At the same time, the centers of primary particles stay in the same position. The second phenomenon, i.e. the densification, encloses all processes that cause the investigated geometries to become more compact. In other words, the centers of primary particles are moved closer to one another.[4]

- **Adhesion:** A sample, advanced model can be found in the paper by Eggersdorfer et al.[5,6] However, in this work only connections that can be easily implemented in large fractal-like aggregate models were investigated. One of the suitable models was introduced in the previous work by Skorupski et al.[7,8] and defined as follows:

$$Y_a = \frac{r_c}{r_p}, \tag{2}$$

  where Y_a is the dimensionless neck size parameter, r_p stands for the radius of the smaller particle and r_c is the radius of the minimum cross section of the investigated neck*. Although this definition is useful and

email: krzysztof.skorupski@pwr.edu.pl

*This definition is valid for various connectors which can be described as a surface of revolution. A more detailed description of the neck size factor Y_a can be found elsewhere.[8]

Optical Modeling and Performance Predictions IX, edited by Mark A. Kahan, Marie B. Levine-West, Proc. of SPIE Vol. 10374, 103740N · © 2017 SPIE · CCC code: 0277-786X/17/$18
doi: 10.1117/12.2273200

relatively simple, a few drawbacks exist. For example, when Y_a is small the connection is almost negligible. Similarly, when primary particles do intersect, even larger values of Y_a have absolutely no impact on the investigated geometry (the volume transfer is non-existent). In this paper, to solve these problems, a new definition was proposed. It is solely based on the amount of the volume transferred. Similarly to Y_a, its value varies from $A = 0$ to $A = 1$. However, it can be used with any connection type. The equation is defined as follows:

$$A = V_c/V_m. \tag{3}$$

The idea behind it is simple - V_c is the total neck volume (excluding the internal assembly of primary particles, regardless of their size, shape, and mutual interactions) and V_m is the volume that would be transferred if the connection reached its maximum size (what is presented in Fig. 1). Note, that this model does not neglect obstacles that can modify the shape of the connection.

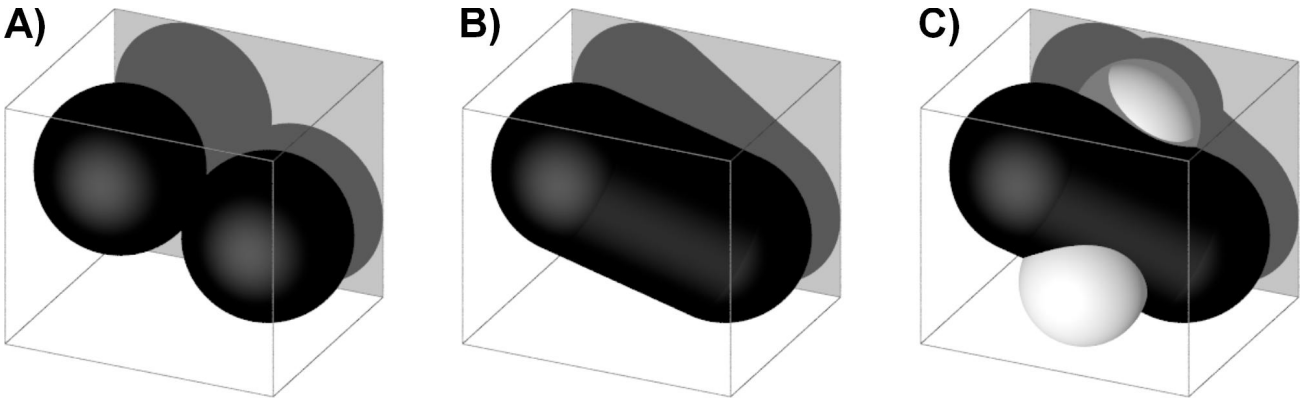

Figure 1. A) Two primary particles in point contact; $A = 0$, B) Two primary particles and a full neck; $A = 1$, C) Two primary particles, a full neck, and two elements affecting the size of the neck (the volume transfer is diminished); $A = 1$.

- **Densification:** A sample model introduced by Brasil et al.[9] (which has already been used in various projects[8,10–12]) is defined as follows[†]:

$$C_b = 1 - \frac{l}{2r_p}, \tag{4}$$

where l is the distance between the centers of two monodisperse primary particles with the radius r_p. The equation can be extended to large fractal-like aggregates where polydispersity is relatively small (in such a case $2r_p$ changes to $r_{p1} + r_{p2}$). However, once again, a few problems arise. For example, when two primary particles are characterized by a different size, one of them can be positioned inside the second one. In such a case C_b could be close to zero, indicating that the particles intersect only slightly (what is not true). Furthermore, when two primary particles are in the same position and their shapes are very different, the overlap factor reaches $C_b = 1$. However, their shapes can still be clearly distinguishable, what is presented in Fig. 2. A different approach is to move particle centers to the geometric center of the investigated geometry by a specific distance. $C_a = 1$ means that the initial geometry was not altered and $C_a = 1$ indicates that all particles were moved to the same point (i.e. the geometric center). This behavior can be described by the equation:

$$\vec{r}_{pi}* = C_a \cdot \vec{r}_{pi}, \tag{5}$$

where $\vec{r}_{pi}$ is the position of the i-th primary particle with respect to the geometric center of the investigated geometry. $\vec{r}_{pi}*$ is the position of the same particle after implementing the shrinkage procedure. Still, this definition does not take into consideration the particle size and shape. Furthermore, it does not provide the initial overlap level of the investigated geometry (i.e. when C_a reaches zero it does not mean that

[†]A similar model was proposed by Oh and Sorensen.[13]

C_b is zero as well[‡]). On the other hand, it is very easy to implement the shrinking procedure using this definition. In this work a new densification (overlap) parameter, based on the volume V, was introduced. The equation is defined as follows:

$$D = V_d/V_a, \tag{6}$$

where V_d is the overlap volume and V_a denotes the volume of the smaller particle. Note, that only the overlap level between two particles can be measured. Therefore, when one of them is inside a more complex geometry, all touching elements are considered to be one particle (what is presented in Fig. 2).

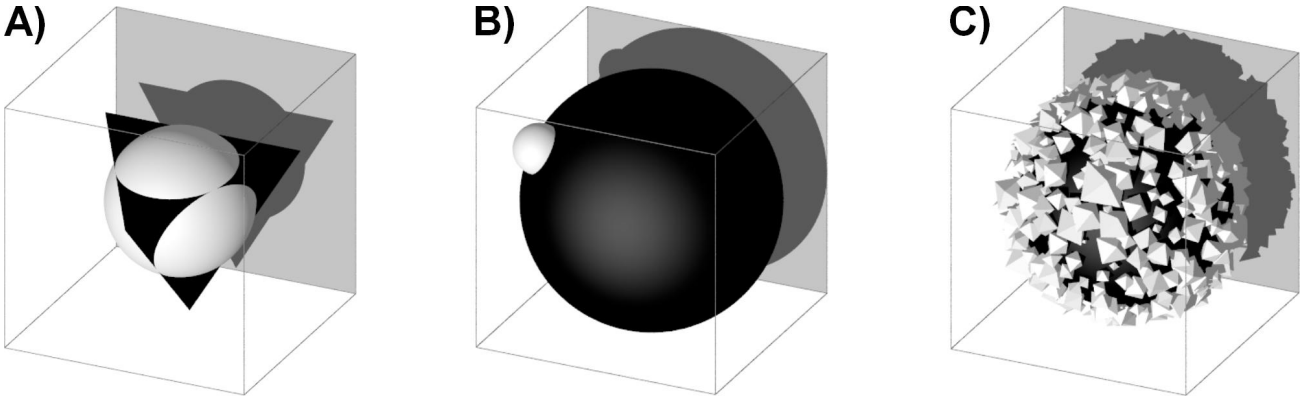

Figure 2. A) Two primary particles in the same position; $C_a = 1$, $C_b = 1$, $D \neq 1$, B) Two intersecting primary particles with different size; $C_a \approx 0$, $C_b \approx 0$, $D \neq 0$, C) A set of intersecting particles. All white particles are in contact with the core (black) particle, and therefore, are considered to be a single particle as well.

The relations between old (C_a, Y_a) and new (D, A) parameters are presented in Fig. 3. To measure the neck level or the overlap level for a fractal-like aggregate, all possible connections/necks must be investigated and measured values must be averaged. A combination of the introduced parameters can be used to model various stages of the sintering process.[14–17]

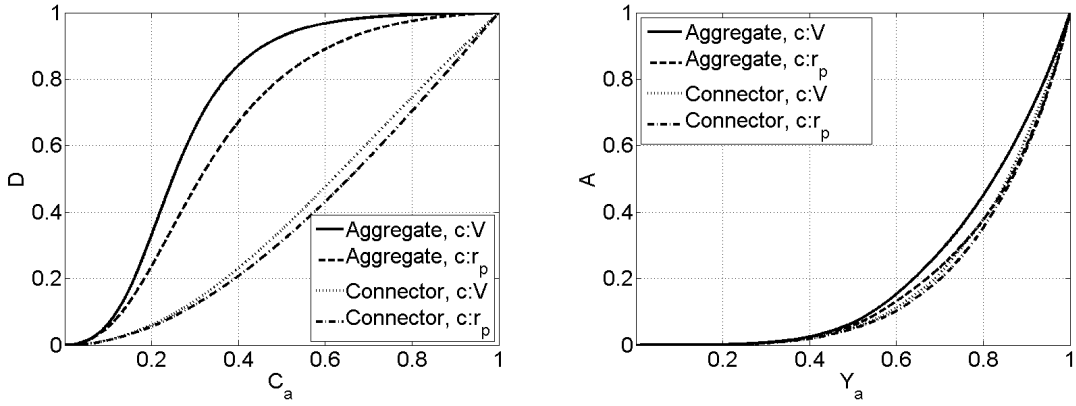

Figure 3. The relation C_a - D and Y_a - A. Two cases are presented: when the volume is constant ($c : V$) and when the particle radius remains unchanged ($c : r_p$). Calculations were made for a single cylindrical connector and a fractal-like aggregate.

[‡]However, when $C_b = C_a = 0$ is true for the initial geometry (the investigated monodisperse aggregate model is composed of primary particles in point contact), all changes made to one parameter are reflected in the second one, i.e. $C_b \approx C_a$.

2. LIGHT SCATTERING SIMULATIONS

To prove that an alteration of the two introduced parameters, namely D and A, have an undeniable impact on the optical properties of fractal-like aggregates, light scattering simulations were performed. This technique has been successfully used to determine morphological parameters of various geometries, like erythrocytes, fibres, etc.[18–23] In this work, two geometries were investigated: a single cylindrical connector between two WO_3 particles, and a fractal-like aggregate composed of polydisperse primary particles. For the extensive simulations the ADDA algorithm, which is based on the DDA (Discrete Dipole Approximation) method was used.[24–28] The incident wavelength varied from $\lambda = 400nm$ to $\lambda = 800nm$ with the step $\Delta\lambda = 50nm$. All results were averaged using the Romberg integration technique in the adaptive regime and the maximum number of orientations was 256.[29,30] The distance between volume elements (dipoles) was $d = 2nm$. The volume correction procedure was not implemented. The polarizability expression was IGT:SO (approximate Integration of Green's Tensor over the dipole). The complex refractive index of WO_3 was adapted from the paper by Vourdas et al.[31] and is presented in Fig. 4. To prove that the aforementioned settings were valid, a comparison of the resulting extinction cross section

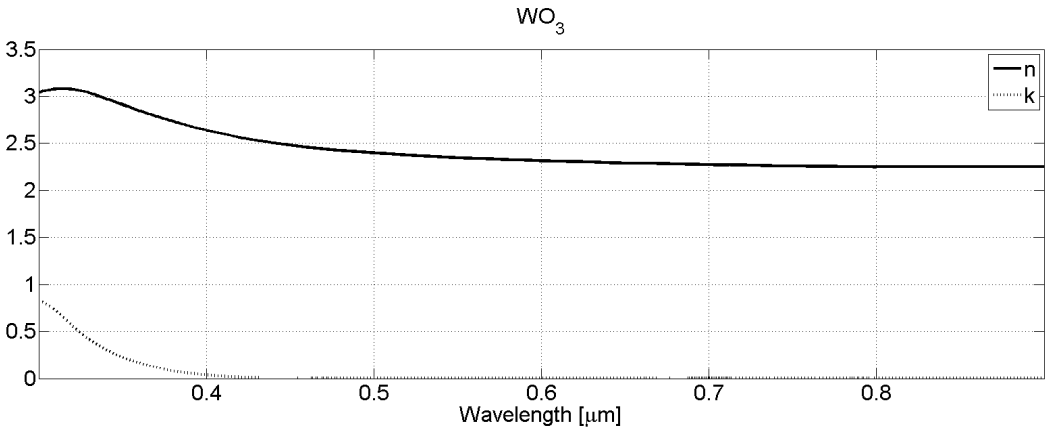

Figure 4. The complex refractive index m for WO_3 adapted from the work by Vourdas et al.[31]

C_{ext} with the results, calculated using a different scattering method, namely T-Matrix, was performed.[32–35] One additional geometry used in this study was a sphere characterized by an equivalent volume to the investigated WO_3 aggregate. The resulting extinction cross section C_{ext} for all geometries is presented in Fig. 5. In the same figure, the relative extinction error δC_{ext} for the two methods (ADDA, T-Matrix) is shown. The relative extinction error δC_{ext} could be additionally boosted by the fact that algorithms use slightly different averaging procedures.

2.1 Cylindrical connectors

For this part of the study a cylindrical connector between two WO_3 primary particles with the radius $r_p = 20nm$ was generated. The changes of D and A are presented in Fig. 6 and Fig. 7 respectively. The relative extinction error δC_{ext} is presented in Fig. 8 and in Fig. 9. As the reference, the geometry without any necks and intersections was used (i.e. $A = 0$, $D = 0$). In the first case, the volume of the geometry V was always constant. This means that, after increasing the size of the neck or using the shrinking procedure, r_p was adapted accordingly. In the second case, r_p was not modified. This shows what might happen when necks exist, but are excluded from the aggregate model. Fig. 10 presents the changes of D when A is at its maximum level. The results prove that, as expected, necking has an important impact on light scattering simulations. The changes are especially visible when the volume of the geometry V is not conserved. The increase of V results in an immediate increase of the extinction cross section C_{ext}.

2.2 Fractal-like aggregates

The WO_3 aggregate model was composed of $N_p = 50$ primary particles. The parameters used for its generation were as follows: geometric mean $\bar{r}_p = 20nm$, the geometric standard deviation $\sigma r_p = 1.2nm$. The fractal

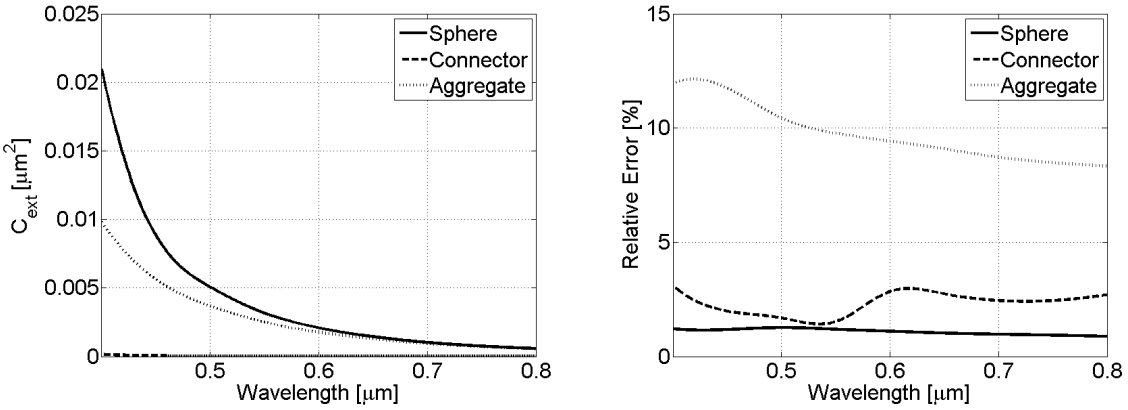

Figure 5. Left) The extinction cross section C_{ext} calculated for the investigated geometries. Right) The difference in the extinction cross section C_{ext} between two algorithms, namely ADDA and T-Matrix.

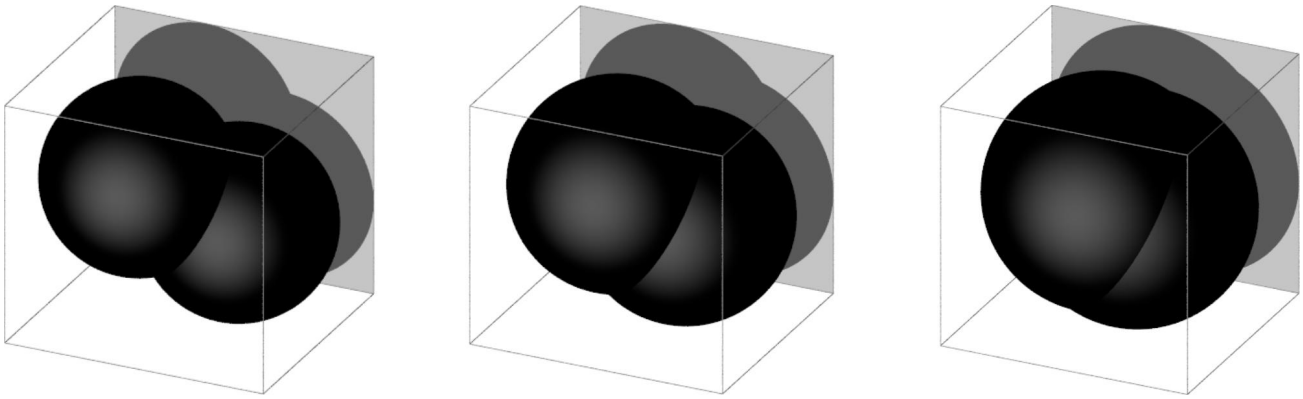

Figure 6. Cylindrical connector - Three geometries characterized by a different value of the densification factor ($D \approx 0.25$, $D \approx 0.50$, $D \approx 0.75$).

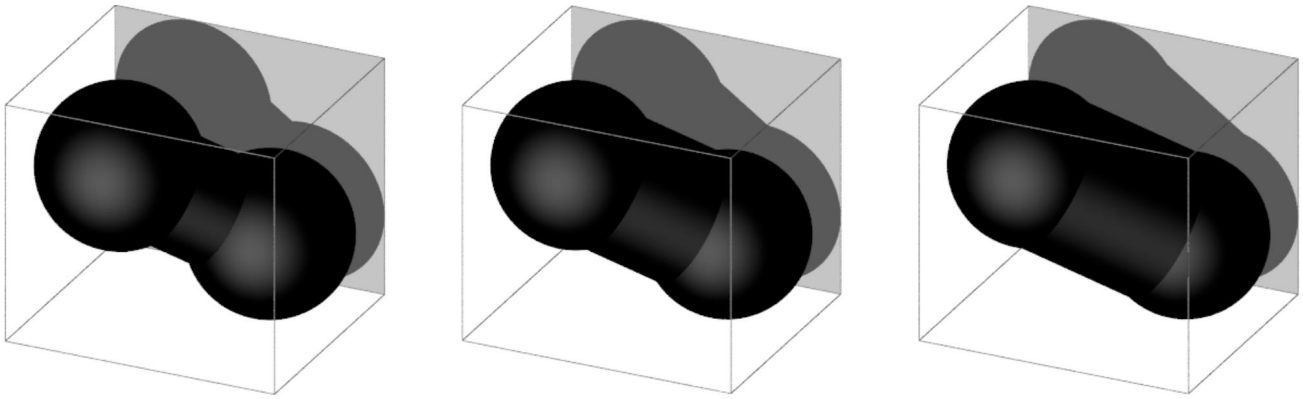

Figure 7. Cylindrical connector - Three geometries characterized by a different value of the adhesion factor ($A \approx 0.25$, $A \approx 0.50$, $A \approx 0.75$).

parameters were $D_f = 1.8$ and $k_f = 1.3$ respectively.[36–39] Note, that these values may vary across different publications. In general, many different techniques for retrieving morphological parameters are available and and each of them might result in slightly different outcome.[10,11,40–51] The geometry was created using the modified CC method described in the paper by Filippov et al.[52] and Skorupski et al.[53] The changes of D and A are

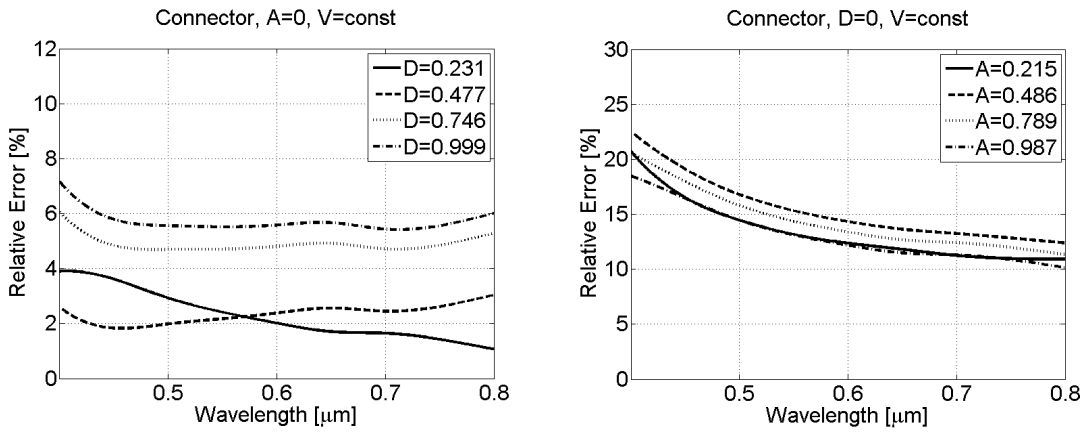

Figure 8. Cylindrical connector - The impact of the densification factor D and the adhesion factor A on the results when the volume of the investigated geometry V is constant.

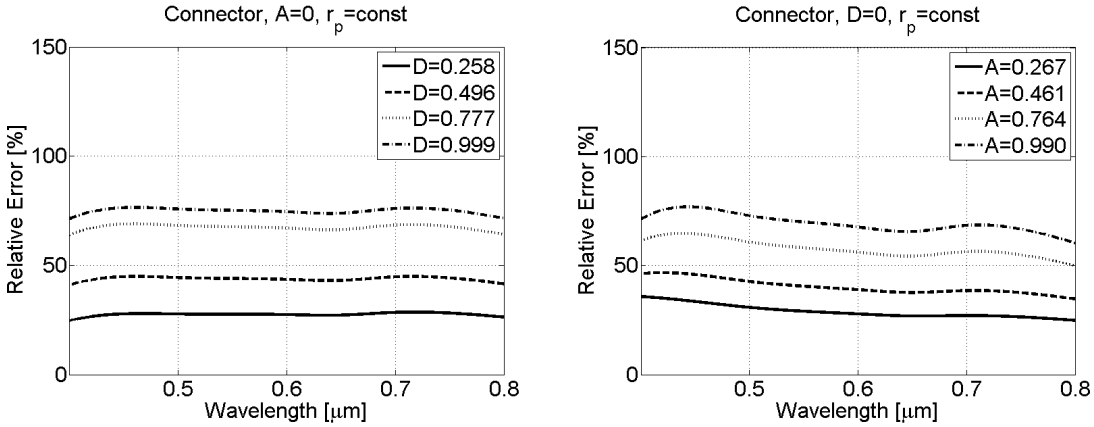

Figure 9. Cylindrical connector - The impact of the densification factor D and the adhesion factor A on the results when the particle radius r_p is constant.

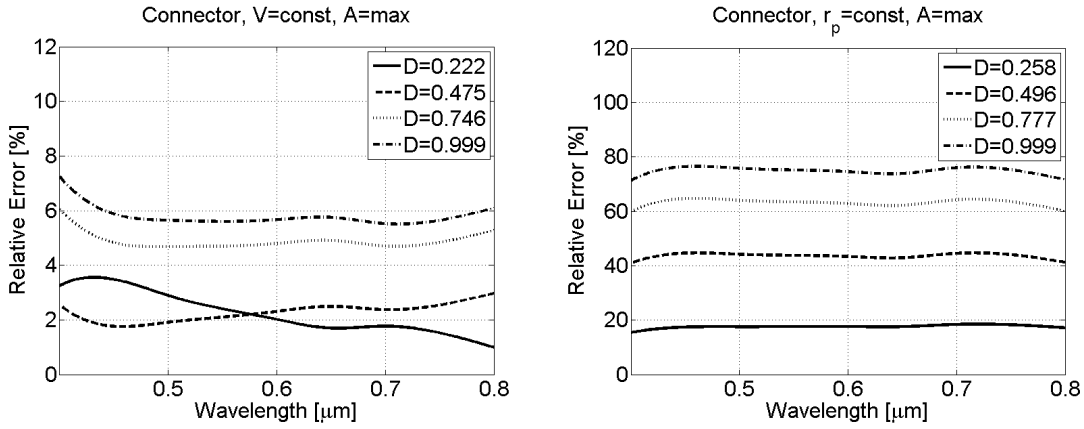

Figure 10. Cylindrical connector - The impact of the densification factor D when the adhesion factor A is at its maximum level.

presented in Fig. 11 and Fig. 12. The results of the light scattering simulations are shown in Fig. 13, Fig. 14 and Fig. 15.

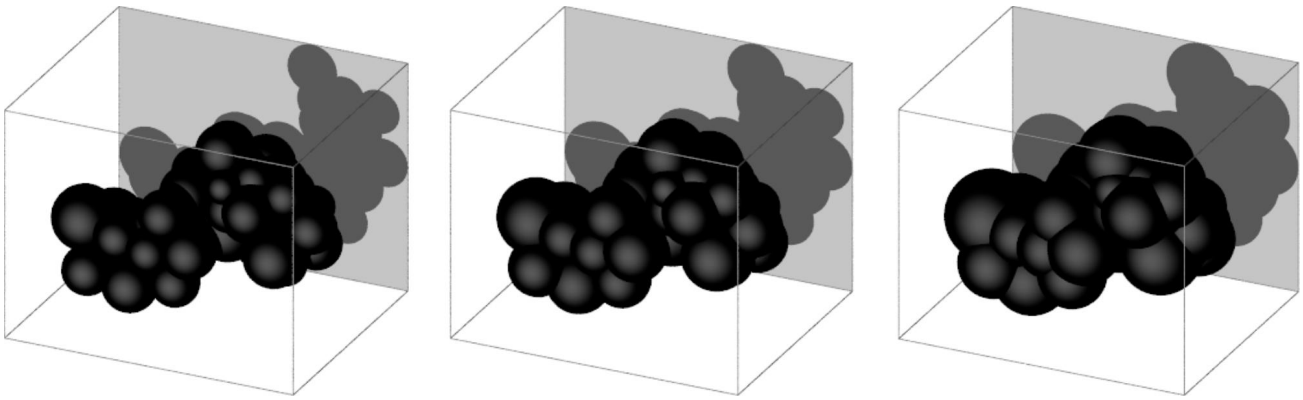

Figure 11. Fractal-like aggregate - Three geometries characterized by a different value of the densification factor ($D \approx 0.25$, $D \approx 0.50$, $D \approx 0.75$).

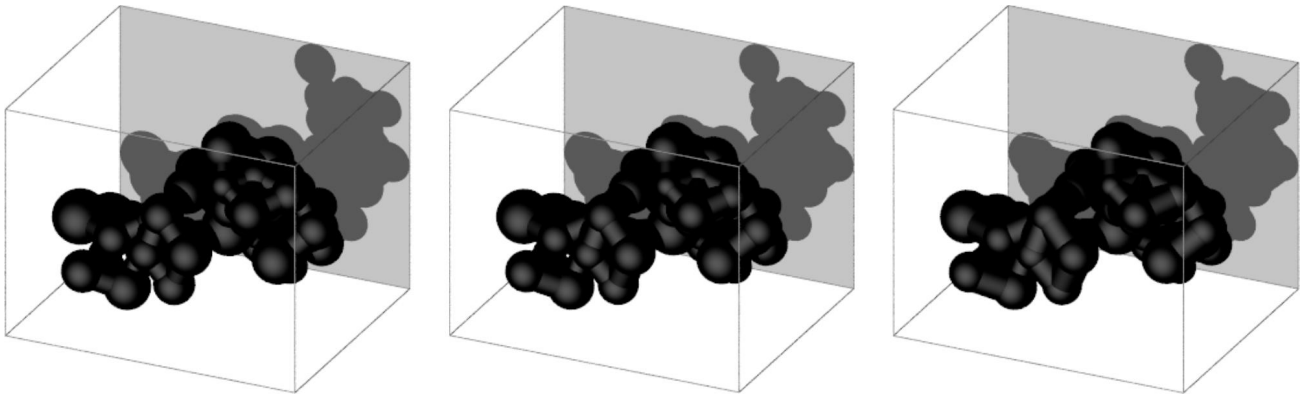

Figure 12. Fractal-like aggregate - Three geometries characterized by a different value of the adhesion factor ($A \approx 0.25$, $A \approx 0.50$, $A \approx 0.75$).

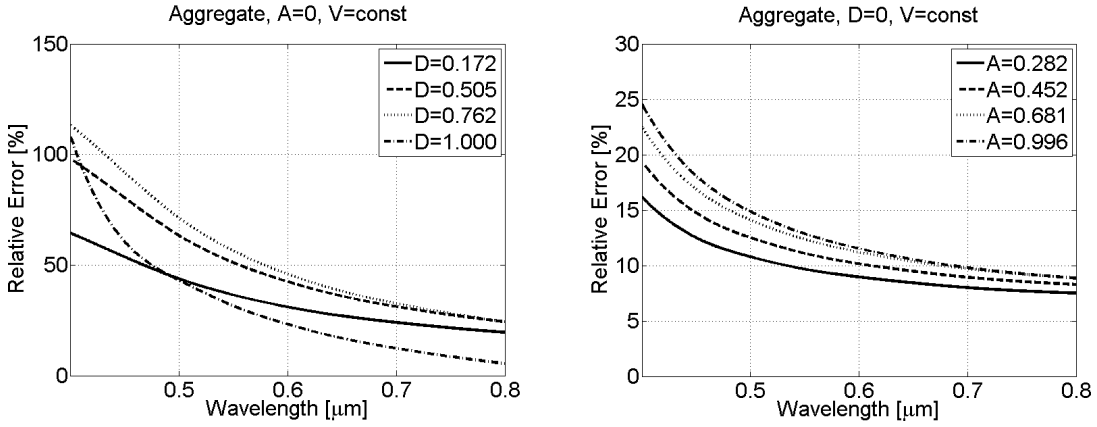

Figure 13. Fractal-like aggregate - The impact of the densification factor D and the adhesion factor A on the results when the volume of the investigated geometry V is constant.

The results once again prove that necking has huge impact on the light scattering results. The increase in the aggregate volume V affects the extinction cross section C_{ext}

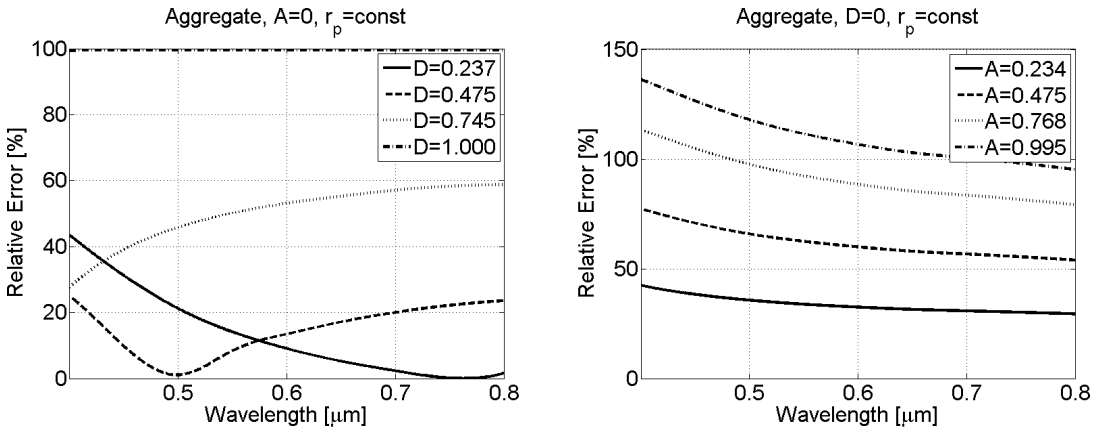

Figure 14. Fractal-like aggregate - The impact of the densification factor D and the adhesion factor A on the results when the particle radius r_p is constant.

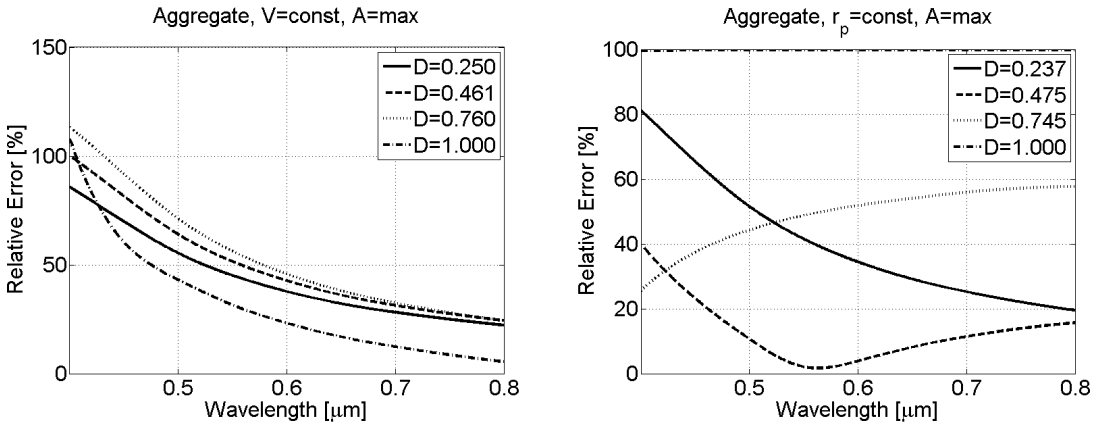

Figure 15. Fractal-like aggregate - The impact of the densification factor D when the adhesion factor A is at its maximum level.

3. CONCLUSIONS

In the paper two parameters for modeling the densification phenomenon D and the adhesion phenomenon A were introduced. Both of them are based on the geometry volume V and can be used with any aggregate type. Furthermore, the study shows that these two parameters have an undeniable impact on the extinction cross section C_{ext} of WO_3 fractal-like aggregates. Complex necks and particle intersections should not be removed from fractal-like aggregate models to improve the quality of simulations.[54]

4. ACKNOWLEDGEMENT

This work is supported by the Polish Ministry of Science and Higher Education, Project No. 0401/0168/16.

REFERENCES

[1] Mandelbrot, B., [*The Fractal Geometry of Nature*], W. H. Freeman and Co. (1982).
[2] Sorensen, C. M., "Light scattering by fractal aggregates: A review," *Aerosol Science and Technology* **35**, 648–687 (2001).
[3] Meakin, P., "A historical introduction to computer models for fractal aggregates," *Journal of Sol-Gel Science and Technology* **15**, 97–117 (1999).

[4] Shimosaka, A., Ueda, Y., Shirakawa, Y., and Hidaka, J., "Sintering mechanism of two spheres forming a homogeneous solid solubility neck," *KONA* **21**, 219–233 (2003).

[5] Eggersdorfer, M. L., Kadau, D., Herrmann, J. H., and Pratsinis, S. E., "Multiparticle sintering dynamics: From fractal-like aggregates to compact structures," *Langmuir* **27**, 6358–6367 (2011).

[6] Eggersdorfer, M. L., Kadau, D., Herrmann, J. H., and Pratsinis, S. E., "Aggregate morphology evolution by sintering: Number and diameter of primary particles," *Aerosol Science and Technology* **46**, 7–19 (2012).

[7] Skorupski, K., Hellmers, J., Feng, W., Mroczka, J., Wriedt, T., and Mdler, L., "Influence of sintering necks on the spectral behaviour of ITO clusters using the discrete dipole approximation," *Journal of Quantitative Spectroscopy and Radiative Transfer* **159**, 11–18 (2015).

[8] Skorupski, K., Mroczka, J., Riefler, N., Oltmann, H., Will, S., and Wriedt, T., "Effect of the necking phenomenon on the optical properties of soot particles," *Journal of Quantitative Spectroscopy and Radiative Transfer* **141**, 40–48 (2014).

[9] Brasil, A., Farias, T., Carvalho, G., and Koylu, U., "Numerical characterization of the morphology of aggregated particles," *Journal of Aerosol Science* **32**, 489–508 (2001).

[10] Brasil, A., Farias, T., and Carvalho, G., "A recipe for image characterization of fractal-like aggregates," *Journal of Aerosol Science* **30**, 1379–1389 (1999).

[11] Oltmann, H., Reimann, J., and Will, S., "Single-shot measurement of soot aggregate sizes by wide-angle light scattering (WALS)," *Applied Physics B: Lasers and Optics* **106**, 171–183 (2012).

[12] Skorupski, K., Mroczka, J., Riefler, N., Oltmann, H., Will, S., and Wriedt, T., "Impact of morphological parameters onto simulated light scattering patterns," *Journal of Quantitative Spectroscopy and Radiative Transfer* **119**, 53–66 (2013).

[13] Oh, C. and Sorensen, C. M., "The effect of overlap between monomers on the determination of fractal cluster morphology," *Journal of Colloid and Interface Science* **193**, 17–25 (1997).

[14] Buesser, B., Groehn, A. J., and Pratsinis, S. E., "Sintering rate and mechanism of TiO2 nanoparticles by molecular dynamics," *The Journal of Physical Chemistry C* **115**, 11030–11035 (2011).

[15] Schmid, H. J., Tejwani, S., Artelt, C., and Peukert, W., "Monte carlo simulation of aggregate morphology for simultaneous coagulation and sintering," *Journal of Nanoparticle Research* **6**, 613–626 (2004).

[16] Hellmers, J., Riefler, N., Wriedt, T., and Eremin, Y. A., "Light scattering simulation for the characterization of sintered silver nanoparticles," *Journal of Quantitative Spectroscopy and Radiative Transfer* **109**, 1363–1373 (2008).

[17] Hellmers, J. and Wriedt, T., "Applicability of t-matrix light scattering simulations for the spectral investigation of sintered nanoparticles," *Journal of Quantitative Spectroscopy and Radiative Transfer* **123**, 53–61 (2013).

[18] Wriedt, T., Hellmers, J., Eremina, E., and Schuh, R., "Light scattering by single erythrocyte: Comparison of different methods," *Journal of Quantitative Spectroscopy and Radiative Transfer* **100**, 444–456 (2006).

[19] Nilsson, A., Alsholm, P., Karlsson, A., and Andersson-Engels, S., "T-matrix computations of light scattering by red blood cells," *Applied Optics* **37**, 2735–2748 (2000).

[20] Mroczka, J. and Wysoczanski, D., "Plane-wave and gaussian-beam scattering on an infinite cylinder," *Optical Engineering* **39**, 736–770 (2000).

[21] Girasole, T., Gouesbet, G., Grehan, G., Toulouzan, J. L., Mroczka, J., Ren, K., and Wysoczanski, D., "Cylindrical fibre orientation analysis by light scattering. part ii: Experimental aspects," *Particle and Particle Systems Characterization* **14**, 211–218 (1997).

[22] Girasole, T., Bultynck, H., Gouesbet, G., Toulouzan, J. L., Mroczka, J., Ren, K., and Wysoczanski, D., "Cylindrical fibre orientation analysis by light scattering. part i: Numerical aspects," *Particle and Particle Systems Characterization* **14**, 163–174 (1997).

[23] Girasole, T., Toulouzan, J. L., Mroczka, J., and Wysoczanski, D., "Fiber orientation and concentration analysis by light scattering: Experimental setup and diagnosis," *Review of Scientific Instruments* **68**, 2805–2811 (1997).

[24] Yurkin, M. and Hoekstra, A., "The discrete dipole approximation: An overview and recent developments," *Journal of Quantitative Spectroscopy and Radiative Transfer* **106**, 558–589 (2007).

[25] Yurkin, M. and Hoekstra, A., "The discrete-dipole-approximation code ADDA: Capabilities and known limitations," *Journal of Quantitative Spectroscopy and Radiative Transfer* **112**, 2234–2247 (2011).

[26] Draine, B. T. and Flatau, P. J., "User guide for the discrete dipole approximation code ddscat 7.2," *Instrumentation and Methods for Astrophysics* (2012).

[27] Draine, B. T. and Flatau, P. J., "Discrete dipole approximation for scattering calculations," *Journal of the Optical Society of America A* **11**, 1491–1499 (1994).

[28] Penttila, A., Zubko, E., Lumme, K., Muinonen, K., Yurkin, M., Draine, B., Rahola, J., Hoekstra, A., and Shkuratov, Y., "Comparison between discrete dipole implementations and exact techniques," *Journal of Quantitative Spectroscopy and Radiative Transfer* **106**, 417–436 (2007).

[29] Davis, P. J. and Rabinowitz, P., [*Methods of Numerical Integration*], New York: Academic Press (1975).

[30] Riefler, N., Stasio, S., and Wriedt, T., "Structural analysis of clusters using configurational and orientational averaging in light scattering analysis," *Journal of Quantitative Spectroscopy and Radiative Transfer* **89**, 323–342 (2004).

[31] Vourdas, N., Dalamagkidis, K., Kostis, I., Vasilopoulou, M., and Davazoglou, D., "Omnidirectional antireflective properties of porous tungsten oxide films with in-depth variation of void fraction and stoichiometry," *Optics Communications* **285**, 5229–5234 (2012).

[32] Waterman, P. C., "Symmetry, unitarity and geometry in electromagnetic scattering," *Physical Review D* **3**, 825–839 (1971).

[33] Mishchenko, M. I., Travis, L. D., and Mackowski, D. W., "T-matrix computations of light scattering by nonspherical particles: a review," *Journal of Quantitative Spectroscopy and Radiative Transfer* **55**, 535–575 (1996).

[34] Mishchenko, M. I. and Travis, L. D., "Capabilities and limitations of a current fortran implementation of the t-matrix method for randomly oriented, rotationally oriented symetric scatters," *Journal of Quantitative Spectroscopy and Radiative Transfer* **60**, 309–324 (1998).

[35] Mackowski, D. and Mischenko, M., "A multiple sphere t-matrix fortran code for use on parallel computer clusters," *Journal of Quantitative Spectroscopy and Radiative Transfer* **112**, 2182–2192 (2011).

[36] Arutanti, O., Ogi, T., Nandiyanto, A. B. D., Iskandar, F., and Okuyama, K., "Controllable crystallite and particle sizes of WO3 particles prepared by a spray-pyrolysis method and their photocatalytic activity," *American Institute of Chemical Engineers Journal* **60**, 41–49 (2014).

[37] Poluboyarov, V. A., Korotaeva, Z. A., and Andryushkova, O. A., "Preparation of ultrafine particles by mechanical processing," *Inorganic Materials* **37**, 592–595 (2001).

[38] Amano, F., Ishinaga, E., and Yamakata, A., "Effect of particle size on the photocatalytic activity of WO3 particles for water oxidation," *The Journal of Physical Chemistry C* **117**, 22584–22590 (2013).

[39] Kozan, M., Thangala, J., Bogale, R., Menguc, M. P., and Sunkara, M. K., "In-situ characterization of dispersion stability of WO3 nanoparticles and nanowires," *Journal of Nanoparticle Research* **10**, 599–612 (2008).

[40] Mroczka, J. and Szczuczyski, D. K., "Inverse problems formulated in terms of first-kind fredholm integral equations in indirect measurements," *Metrology and Measurement Systems* **16**, 333–357 (2009).

[41] Mroczka, J. and Szczuczyski, D. K., "Improved regularized solution of the inverse problem in turbidimetric measurements," *Applied Optics* **5**, 4591 (2010).

[42] Mroczka, J. and Szczuczyski, D. K., "Problem odwrotny - jako rekonstrukcji funkcji rozkadu wielkoci czstek w pomiarach nefelometrycznych i turbidymetrycznych," *PAK* **9**, 246–249 (2007).

[43] Mroczka, J. and Szczuczyski, D. K., "Simulation research on improved regularized solution of the inverse problem in spectral extinction measurements," *Applied Optics* **51**, 1715–1723 (2012).

[44] Mroczka, J., Wozniak, M., and Onofri, F. R. A., "Algorithms and methods for analysis of the optical structure factor of fractal aggregates," *Metrology and Measurements Systems* **19**, 459–470 (2012).

[45] Will, S., Schraml, S., Bader, K., and A.Leipertz, "Performance characteristics of soot primary particle size measurements by time-resolved laser-induced incandescence," *Applied Optics* **37**, 5647–5658 (1998).

[46] Iuliis, S. D., Cignoli, F., and Zizak, G., "Two-color laser-induced incandescence (2C-LII) technique for absolute soot volume fraction measurements in flames," *Applied Optics* **44**, 7–8 (2005).

[47] Ryser, R., Gerber, T., and Dreier, T., "Soot particle sizing during high-pressure diesel spray combustion via time-resolved laser-induced incandescence," *Combustion and Flame* **156**, 120–129 (2009).

[48] Oltmann, H., Reimann, J., and Will, S., "Wide-angle light scattering (WALS) for soot aggregates characterization," *Combustion and Flame* **157**, 516–522 (2010).

[49] Wozniak, M., Onofri, F. R. A., Barbosa, S., Yon, J., and Mroczka, J., "Comparison of methods to derive morphological parameters of multi-fractal samples of particle aggregates from TEM images," *Journal of Aerosol Sciance* **47**, 12–26 (2012).

[50] Czerwinski, M., Mroczka, J., Girasole, T., Gouesbet, G., and Grehan, G., "Light-transmittance predictions under multiple-light-scattering conditions. i. direct problem: hybrid-method approximation," *Applied Optics* **40**, 1514–1524 (2001).

[51] Czerwinski, M., Mroczka, J., Girasole, T., Gouesbet, G., and Grehan, G., "Light-transmittance predictions under multiple-light-scattering conditions. ii. inverse problem: particle size determination," *Applied Optics* **40**, 1525–1531 (2001).

[52] Filippov, A., Zurita, M., and Rosner, D., "Fractal-like aggregates: Relation between morphology and physical properties," *Journal of Colloid and Interface Science* **229**, 261–273 (2000).

[53] Skorupski, K., Mroczka, J., Wriedt, T., and Riefler, N., "A fast and accurate implementation of tunable algorithms used for generation of fractal-like aggregate models," *Physica A: Statistical Mechanics and its Applications* **404**, 106–117 (2014).

[54] Mroczka, J., "The cognitive process in metrology," *Measurements* **46**, 2896–2907 (2013).